Interfacial Binding of Divalent Cations to Calixarene-Based Langmuir Monolayers

Journal:	*Langmuir*
Manuscript ID:	la-2015-00262v
Manuscript Type:	Article
Date Submitted by the Author:	22-Jan-2015
Complete List of Authors:	Tulli, Ludovico Giuseppe; FHNW, Wang, Wenjie; Ames Laboratory, Lindemann, William; Ames Laboratory, MSE Kuzmenko, Ivan; Argonne National Lab, Meier, Wolfgang; University of Basel, Department of Chemistry Vaknin, David; Iowa State University, Ames Laboratory and Physics Shahgaldian, Patrick; Univ. of Applied Sciences NW Switzerland, Inst. of Chemistry and Bioanalytics

Interfacial Binding of Divalent Cations to Calixarene-Based Langmuir Monolayers

Ludovico G. Tulli,[†] Wenjie Wang,[‡] William R. Lindemann,[‡] Ivan Kuzmenko,[§] Wolfgang Meier,[#] David Vaknin[‡] and Patrick Shahgaldian[,†]*

[†]Institute of Chemistry and Bioanalytics, School of Life Science, University of Applied Sciences and Arts Northwestern Switzerland, Muttenz, Switzerland

[‡]Ames Laboratory, and Department of Physics and Astronomy, Iowa State University, Ames, United States

[§] Advanced Photon Source, Argonne National Laboratory, Lemont, Illinois, United States

[#]Department of Chemistry, University of Basel, Switzerland

KEYWORDS: calix[4]arenes, Langmuir monolayers, self-assembly, X-ray near-total-reflection fluorescence, grazing incidence X-ray diffraction.

ABSTRACT

The interactions of Langmuir monolayers produced through the self-assembly of an amphiphilic *p*-carboxy-calix[4]arene (**1**) with a series of divalent, fourth-period transition-metals, at the air-water interface, were investigated. Changes in the interfacial behavior of **1** in response to the presence of $CuCl_2$, $CoCl_2$, $MnCl_2$ and $NiCl_2$ were studied by means of Langmuir compression isotherms and Brewster angle microscopy (BAM). The measurements revealed that the self-assembly properties of **1** are significantly affected by Cu^{2+} ions. The interactions of **1**-based monolayers with Co^{2+} and Cu^{2+} ions were further investigated by means of synchrotron radiation-based X-ray reflectivity (XRR), X-ray near-total-reflection fluorescence (XNTRF), and grazing incidence X-ray diffraction (GIXD). XNTRF and XRR analysis revealed that the monolayer of **1** binds more strongly to Cu^{2+} than Co^{2+} ions. In the presence of relatively high concentrations of Cu^{2+} ions in the subphase (1.4×10^{-3} M), XNTRF exhibits anomalous depth profile behavior and GIXD measurements showed considerably strong diffuse scattering. Both measurements suggest the formation of Cu^{2+} clusters contiguous to the monolayer of **1**.

INTRODUCTION

Amphiphiles represent one of the most efficient classes of building blocks for producing large, self-assembled systems.[1-4] The molecular architecture of amphiphiles is known to have a remarkable effect on their self-assembly properties. For instance, amphiphiles with more than one lipophilic chain preferentially form layered structures.[5] While nature favors glycerol-based amphiphiles (*i.e.*, di-acyl-glycero-phospholipids), chemists have access to a greater range of molecular bases to design amphiphiles. Macrocyclic molecules such as cyclodextrins,[6] crown-ethers[7] and calix[n]arenes[8] present the advantage of combining fairly rigid backbones with the possibility of regioselective chemical modifications. Concerning calixarenes, the basket-like conformation of 4-membered ring derivatives, along with the possibility of selectively functionalizing both their upper and lower rims, make these macrocycles attractive building blocks for the design of amphiphilic molecular receptors.

In the past forty years, particular attention was focused on the binding properties of calix[n]arenes towards inorganic ions. Gutsche reported that Rb^+ acts as a template for the high-yield synthesis of *p*-tert-butylcalix[6]arene.[9] However, the first detailed study on cations complexation of these macrocycles was reported by Christensen, where *p-tert*-butylcalix[n]arenes (with n = 4, 6 and 8) were used as selective cation carriers in liquid membranes.[10] The high binding affinity reported was the result of the appropriate size of the macrocycles, along with the cooperative effect of the hydroxyl groups. Subsequently, a large number of reports dealing with ion complexation of calix[n]arene derivatives were published.[11-17]

Calix[n]arenes have also been studied for their ability to self-assemble as Langmuir monolayers at the air-liquid interface.[18-21] The first report on this topic was published by Regen who coined

the concept of *perforated monolayers* referring to thin film composite membranes of calix[6]arene-based surfactants bearing uniform, oriented and adjustable nanopores.[22] Subsequently, the interaction properties of calix[n]arene monolayers with ions at the air-water interface have been investigated. In the first report dealing with the interfacial selective response of calix[n]arene monolayers towards metal ions, published by Shinkai, the interactions of two calix[n]arene ester derivatives with Na^+, Li^+ and K^+ ions were investigated.[23] While the calix[4]arene ester derivative was shown to be selective towards Na^+ ions, the calix[6]arene counterpart was demonstrated to predominantly interact with K^+ ions. In 2001, Shahgaldian and Coleman described the interaction of *p*-dodecanoylcalix[4]arene monolayers with alkali metals and a range of counterions.[24] Interestingly, the monolayer was largely stabilized by the presence of Rb^+ ions in the subphase with a relevant effect of the counterion. It was demonstrated that the interaction capabilities of the monolayers were not only owing to the molecular architecture of the studied amphiphile but also to their self-assembly state at the interface. Subsequently, Baglioni investigated the complexation properties of four calix[8]arene derivatives with alkaline earth metal ions;[25] all studied macrocycles showed the highest selectivity towards Ba^{2+}. In 2005, the same group reported on the interaction of *p*-tert-butylcalix[6]arene and *p*-tert-butylcalix[8]arene monolayers with a range of K^+ salts.[26] The effect of the counterions on the structure of the films was discussed with regard to their position in the Hofmeister series.

In the present manuscript, we report on the interfacial interactions of Langmuir monolayers of 5,11,17,23-tetra-carboxy-25,26,27,28-tetradodecyloxycalix[4]arene (**1**), cf. Figure 1, with a series of divalent, fourth-period transition-metal ions. Langmuir compression isotherms, Brewster angle microscopy (BAM), X-ray reflectivity (XRR), X-ray diffraction at grazing angles

of incidence (GIXD) and X-ray near-total-reflection fluorescence (XNTRF) measurements shed light on the response of the **1**-based monolayer towards Cu^{2+}, Co^{2+}, Ni^{2+} and Mn^{2+} ions.

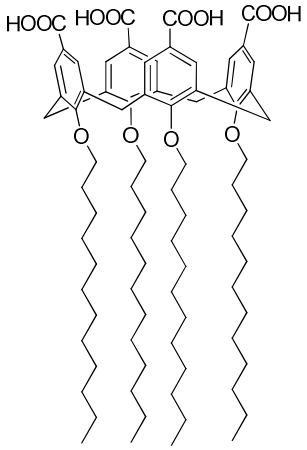

1

Figure 1. Chemical structure of **1**.

EXPERIMENTAL SECTION

Materials. 5,11,17,23-tetra-carboxy-25,26,27,28-tetradodecyloxycalix[4]arene (**1**) was synthesized as previously described, and analytical data (^{1}H and ^{13}C NMR, ES-MS) were in perfect agreement with those previously reported.[27] Analytical grade chloroform and methanol were purchased from Sigma-Aldrich and used without further purification. Nanopure water (resistivity ≥ 18 MΩ cm) was produced using a Millipore Synergy purification system. Copper chloride dihydrate, cobalt chloride hexahydrate, nickel chloride hexahydrate and manganese chloride tetrahydrate were purchased from Sigma-Aldrich and used without further purification.

Langmuir isotherms. Surface pressure-area compression isotherms were carried out using a Nima 112D system. The Langmuir trough was cleaned with analytical grade chloroform and thoroughly rinsed with nanopure water prior to use. Solutions of **1** were prepared by dissolving the appropriate amount of **1** in chloroform (5% methanol) at the concentration of 7.9×10^{-4} mol L^{-1} (1 g L^{-1}). Ten μL of this solution were spread on the water surface using a gas-tight syringe. Monolayers were allowed to stand for 20 minutes to allow for solvent evaporation and stabilization of the amphiphiles at the interface. Symmetric compression of the monolayer was performed at a speed of 5 cm^2 min^{-1}. Aqueous copper chloride, cobalt chloride, nickel chloride and manganese chloride solutions at concentrations of 10^{-5} and 10^{-3} M were prepared extemporaneously by dissolving appropriate amounts of the salts in nanopure water. The accuracies of π_c and A_0 measurements were of ± 1 mN m^{-1} and ± 1 $Å^2$ $molecule^{-1}$, respectively.

Brewster angle microscopy. Micrographs were acquired by using a Nanofilm_ep3 system (Accurion) equipped with an internal, solid-state laser at a wavelength of 658 nm. The images

were acquired using a CCD camera (768 × 562 pixels) and a 10X objective, equipped with an automatic focus scanner yielding 1 μm lateral resolution.

X-ray near-total-reflection fluorescence, X-ray reflectivity and grazing incidence X-ray diffraction. XNTRF, XRR and GIXD measurements were conducted on the liquid surface spectrometer (LSS) at beam line 9ID-C, Advanced Photon Source (APS), Argonne National Laboratory. The experimental details at 9ID-C (APS) have been described in a previous study.[28] A collimated and monochromatic X-ray beam (at energy E = 13.474 keV, wavelength $\lambda = 0.9201$ Å) is steered onto aqueous surfaces at a desired incident angle α_i. The angular dependence of the XNTRF and XRR are expressed as functions of Q_z, the z-component (surface normal) of the scattering vector, where $Q_z = (4\pi \lambda^{-1})\sin \alpha_i$. The fluorescence measurements are conducted near the critical angle for total reflection, α_c (its corresponding Q_z, denoted as Q_c), using an energy dispersive detector (EDD, silicon drift X-ray detector, Vortex-90EX) that subtended the illuminated surface area with a collimator (angular resolution ~ 1º) in the front end of the probe. Various attenuation levels for the incident beam are used depending on the Q_z-range scanned. For a full Q_z-range scan, where α_i varied from below to above the critical angle, the incident beam is attenuated more (to avoid saturation of the EDD) at α_i greater than α_c as a result of intense scattering of the primary beam from bulk solution. The specular reflectivity, R, is measured with a scintillation detector (Bicron) at X-ray exit angle, α_f, and equals to α_i. All X-ray experiments were performed while purging the sealed enclosure of the trough with helium (pre-bubbled in water) to minimize the background scattering from air and potential radiation damage to the sample. GIXD measurements were conducted at $\alpha_i = 0.065°$, below the critical angle, α_c (= 0.091°), for total reflection using through Soller slits and a line detector (Mythen). The GIXD scans displayed here are obtained by integrating the intensities over a certain Q_z range

and displayed as a function of Q_{xy}, where Q_{xy} is the horizontal component (parallel to the surface) of the scattering vector. During the X-ray experiments a tolerance of ± 2 mN m^{-1} from the desired surface pressure of 20 mN m^{-1} was allowed.

RESULTS AND DISCUSSION

The self-assembly properties of **1** on pure water, and aqueous subphases of $CuCl_2$, $CoCl_2$, $NiCl_2$ and $MnCl_2$ salts at concentrations of 10^{-5} and 10^{-3} M were investigated by measuring Langmuir compression isotherms, cf. Figure 2. The counterion, Cl^-, was retained constant to avoid counterion effects as previously observed for *p*-dodecanoylcalix[4]arene.[24] The surface pressure-molecular area isotherm of **1** on pure water shows a collapse pressure (π_c) of 51 mN m^{-1} and a takeoff area (A_0) of 122 $Å^2$ $molecule^{-1}$ (Table 1), in agreement with a densely packed monolayer of a calix[4]arene in the cone conformation, with the pseudo C_4 symmetry axis orthogonal to the air-water interface. In addition, the isotherm reveals the presence of a phase transition at 39 mN m^{-1} suggesting that a molecular rearrangement of the film occurs, consistent with previously reported results.[27]

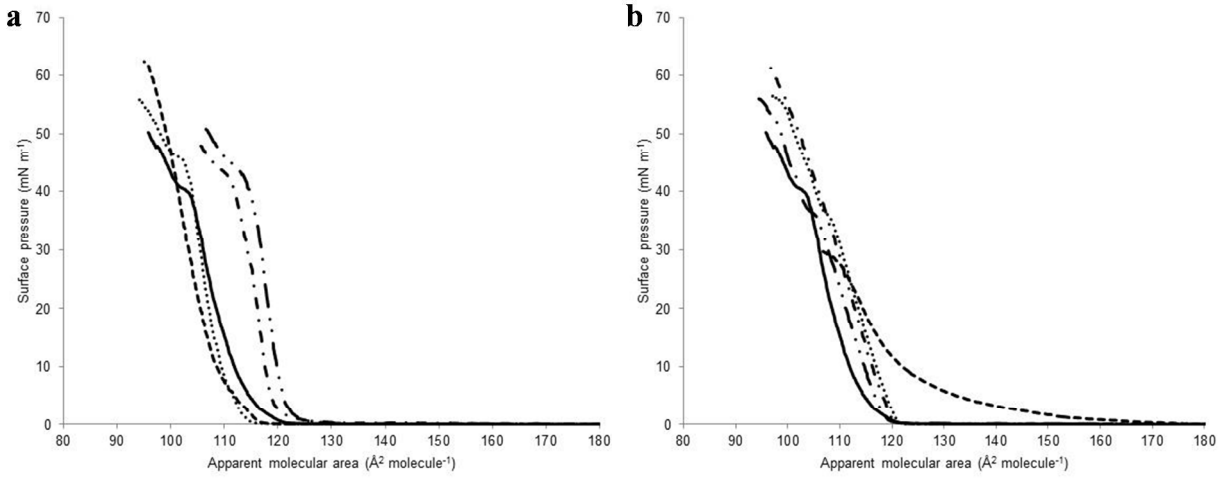

Figure 2. Surface pressure-area isotherms of **1** on pure water (−) and on 10^{-5} M (**a**) and 10^{-3} M (**b**) aqueous $CuCl_2$ (−−), $CoCl_2$ (··), $NiCl_2$ (−·−) and $MnCl_2$ (−···−) solutions.

Table 1. Characteristic values of the isotherms of **1**.

subphase	π_c	A_0	$\lvert\delta\pi/\delta A\rvert$
water	51	122	3.9
$CuCl_2$ (10^{-5} M)	62	116	4.4
$CoCl_2$ (10^{-5} M)	55	113	6.1
$NiCl_2$ (10^{-5} M)	51	126	5.5
$MnCl_2$ (10^{-5} M)	51	125	6.6
$CuCl_2$ (10^{-3} M)	29	174	1.3
$CoCl_2$ (10^{-3} M)	56	121	3
$NiCl_2$ (10^{-3} M)	60	121	2.9
$MnCl_2$ (10^{-3} M)	56	120	2.8

Π_c represents the maximum value of pressure to which, after further compression of the monolayer, the amphiphile is forced out of the interface (i.e., collapse). A_0 is the area occupied by one molecule at the isotherm takeoff. $|\delta\pi/\delta A|$ is the modulus of the slope at the steepest part of the monolayer. Π_c (± 1) values are given in mN m^{-1}, area values (± 1) in $Å^2$ $molecule^{-1}$, $|\delta\pi/\delta A|$ values in mN $m^{-1}/Å^2$ $molecule^{-1}$.

In the presence of 10^{-5} M aqueous $CoCl_2$, $NiCl_2$ and $MnCl_2$ subphases, the collapse pressure (55, 51 and 51 mN m^{-1} respectively) and A_0 (113, 126 and 125 $Å^2$ $molecule^{-1}$ respectively) values are fairly close to that measured on pure water (π_c = 51 mN m^{-1}, A_0 = 122 $Å^2$ $molecule^{-1}$). The rigidity of Langmuir monolayers is typically defined by its compressibility modulus:

$$C_s^{-1} = -A\,\frac{\partial\pi}{\partial A}$$

As the compressibility modulus is directly dependent on the molecular area value, it may be strongly impacted by a shift of the isotherm towards different area values; it is therefore not satisfactory for describing the interactions of a monolayer with an analyte dissolved in the subphase. For this reason, we prefer to use the modulus of the slope of the steepest portion of the isotherm: $|\delta\pi/\delta A|$. The $|\delta\pi/\delta A|$ values of the monomolecular films of **1** on the 10^{-5} M $CoCl_2$, $NiCl_2$, and $MnCl_2$ subphases are 6.1, 5.5, and 6.6 mN $m^{-1}/Å^2$ $molecule^{-1}$ respectively, higher than that measured on pure water ($|\delta\pi/\delta A|$ = 3.9 mN $m^{-1}/Å^2$ $molecule^{-1}$). This increase indicates the stiffening of the monomolecular film in response to the presence of ions and confirms their

interfacial interaction with the polar portion of the monolayer. In the presence of a 10^{-5} M aqueous $CuCl_2$ subphase, the A_0 value slightly decreases from 122 to 116 $Å^2$ molecule^{-1}, while the $|\delta\pi/\delta A|$ slightly increases from 3.9 to 4.4 mN m^{-1}/$Å^2$ molecule^{-1}. In addition, the π_c increases from 51 up to 62 mN m^{-1}, a considerably high value for a monomolecular film formed by a calixarene-based amphiphile. Furthermore, the characteristic phase transition observed on water is absent for Cu^{2+} solution at 10^{-5} M. These observations indicate that Cu^{2+}, Co^{2+}, Ni^{2+} and Mn^{2+} ions interact with the monolayer even at a relatively low concentration of 10^{-5} M.

In a previous work,[27] we showed that, in the solid state, **1** adopts a pinched cone conformation whereby two distal phenyl rings are splayed apart and the other two are closer to each other. The amphiphiles are self-assembled in a bilayered fashion where the carboxylic groups of adjacent macrocycles are arranged side-by-side. In the current case, we postulate that at the air-water interface, in the presence of divalent ions in the aqueous subphase (10^{-5} M), the carboxylic groups of adjacent molecules of **1**, self-assembled as a Langmuir monolayer at the air-water interface, are oriented head-to-head. These carboxylic groups bind the cations with possibly a distorted octahedral coordination geometry, where the ions are coordinated by two carboxylic groups of adjacent amphiphiles, and two water molecules, in *cis* positions around the central ion. The geometric constraints of the ligand and the limited freedom of the *p*-carboxylic functions rule out the presence of a binary 1:1 complex between **1** and the ions. Distorted octahedral coordination geometry for solid-state Cu(II), Co(II), Ni(II) and Mn(II)-carboxylate complexes has been reported in the literature.[29-32] For instance, the crystal structure of $[Cu_2$(biphenyl-4,4'-dicarboxylate$)_2$(1,10-phenanthroline$)_2(H_2O)]_2\cdot 2H_2O$ reported by Chen shows that the distance between the oxygen atoms of two adjacent carboxylic groups that bind the Cu^{2+} ion is 3.2 Å.[32] This distance is slightly higher than the sum of the Van der Waals radii of the two oxygen atoms

that is ~ 3 Å. Therefore, the formation of a distorted octahedral complex with the ions dissolved in the subphase is not expected to cause a relevant increase in the A_0 values of the isotherms of **1**, in agreement with the results obtained by compression isotherms. In the presence of a higher concentration (10^{-3} M) of $NiCl_2$, $MnCl_2$, and $CoCl_2$ subphases, the π_c values of the isotherms of **1** increase from a value of 51 on pure water to 60, 56 and 56 mN m^{-1}. The $|\delta\pi/\delta A|$ values considerably decrease from a value of 3.9 on pure water to 2.9, 2.8 and 3 mN $m^{-1}/Å^2$ $molecule^{-1}$ for Ni^{2+}, Mn^{2+} and Co^{2+} ions respectively. This indicates that, at higher concentrations, the interfacial binding causes the formation of a more expanded monolayer. Interestingly, the isotherms of **1** on 10^{-3} M aqueous $NiCl_2$, $MnCl_2$, and $CoCl_2$ solutions reveal that, at the takeoff (π = 0.1 mN m^{-1}), the surface pressure constantly increases and no further changes in the slope of the isotherms are observed. This suggests that these ions trigger self-assembly of **1** as large domains even prior to compression. For $CuCl_2$ at 10^{-3} M, the isotherm profile of **1** notably changes in comparison with that measured on pure water and on a 10^{-5} M aqueous $CuCl_2$ solution. Indeed, the π_c drops to a value of 29 mN m^{-1} (π_c = 51 mN m^{-1} on pure water and 62 mN m^{-1} on a 10^{-5} M aqueous $CuCl_2$ solution) and the A_0 is shifted up to 168 $Å^2$ $molecule^{-1}$ (A_0 = 122 $Å^2$ $molecule^{-1}$ on pure water and 116 $Å^2$ $molecule^{-1}$ on a 10^{-5} M aqueous $CuCl_2$ solution). In addition, the $|\delta\pi/\delta A|$ value decreases considerably from 3.9 on pure water and 4.4 on a 10^{-5} M to 1.3 mN $m^{-1}/Å^2$ $molecule^{-1}$. The different isotherm profile of **1** on a 10^{-3} M aqueous $CuCl_2$ solution with respect to those on $NiCl_2$, $MnCl_2$, and $CoCl_2$ subphases at the same concentration may be due to the formation of clusters or large aggregates.

The microscopic structures of the monolayer of **1** on pure water, 10^{-5} and 10^{-3} M aqueous $CuCl_2$, $CoCl_2$, $NiCl_2$ and $MnCl_2$ subphases were investigated by means of BAM, as shown in Figure 3.

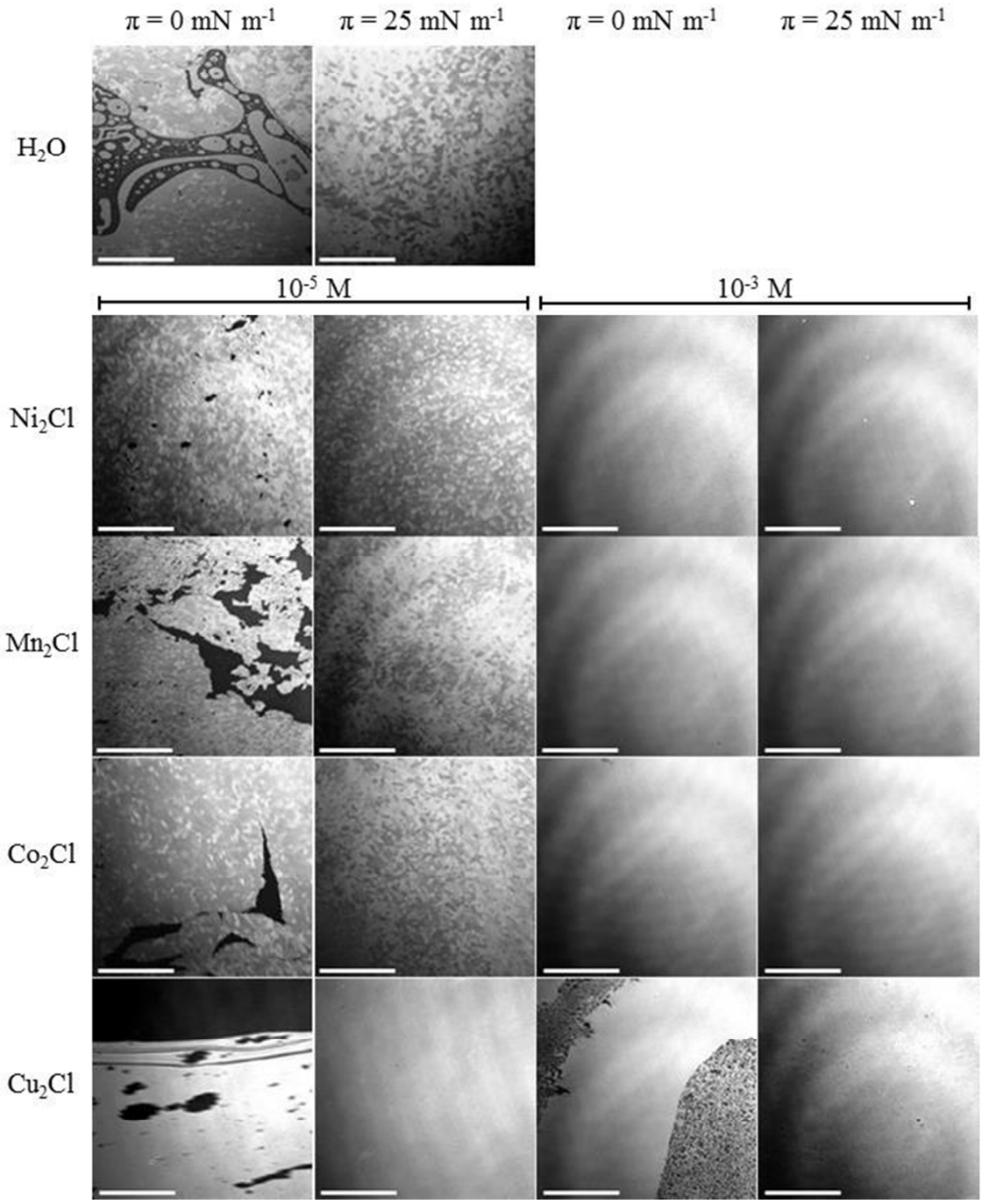

Figure 3. BAM micrographs of the monolayer of **1** on water and on 10^{-5} M and 10^{-3} M aqueous $NiCl_2$, $MnCl_2$, $CoCl_2$ and $CuCl_2$ solutions. Scale bar = 100 μm.

The micrographs of the monolayer of **1** on pure water reveal that, at the isotherm takeoff (π = 0.1 mN m^{-1}), relatively large liquid-condensed domains are formed. Interestingly, while the structure

of the majority of calixarene-based monolayers appears uniform for surface pressures higher than 1 mN m^{-1},[33] the film lacks homogeneity. Indeed, the micrographs show the presence of two types of domains with different contrasts. In the presence of 10^{-5} M aqueous $NiCl_2$, $MnCl_2$ and $CoCl_2$ solutions, the texture of the monolayers appears similar to that on water, with the presence of relatively large liquid-condensed domains observed at the isotherm takeoff (π = 0.1 mN m^{-1}). This morphology is maintained until the collapse of the films (Figure S1). These results indicate that the interfacial interaction of **1** with Ni^{2+}, Mn^{2+} and Co^{2+} does not drastically affect the microscopic structure of the monomolecular film. In contrast, in the presence of Cu^{2+} (10^{-5} M), the morphology of the film noticeably changes in comparison with that on pure water. Indeed, at the isotherm takeoff (π = 0.1 mN m^{-1}), the monolayer appears and remains uniform until collapse (Figure 3 and Figure S2). Interestingly, in the presence of 10^{-3} M aqueous $NiCl_2$, $MnCl_2$ and $CoCl_2$ solutions, a highly homogeneous monolayer is formed before the isotherm takeoff (π = 0 mN m^{-1}). The monolayer of **1** exhibits a uniform phase even when the available molecular area is as high as 140 $Å^2$ $molecule^{-1}$ in the presence of $NiCl_2$, 128 $Å^2$ $molecule^{-1}$ in the presence of $MnCl_2$ and 130 $Å^2$ $molecule^{-1}$ in the presence of $CoCl_2$. These morphologies are maintained until collapse (Figure S3). These results indicate that the interaction of the amphiphile with Co^{2+}, Ni^{2+}, and Mn^{2+} ions causes the formation of condensed monolayers of **1** prior to compression, consistent with our conclusions drawn from the isotherm experiments. In the presence of a 10^{-3} M aqueous $CuCl_2$ solution, the monolayer exhibits an irregular phase that turns homogeneous only at the collapse (Figure 3 and Figure S4), thus confirming that the effect of Cu^{2+} ions on the monolayer of **1** is substantially different from that of the others. In order to gather further insights into the interfacial behavior of **1**, the interactions with Co^{2+} and Cu^{2+} ions were studied

by means of synchrotron-based radiations, XNTRF, XRR, and GIXD by specifically monitoring the accumulation of these ions at the head group template.

The surface fluorescence spectra collected at Q_z = 0.018 Å^{-1}, (below Q_c = 0.0218 Å^{-1}) corresponding to a vertical X-ray penetration depth of ~ 80 Å, are shown in Figure 4.

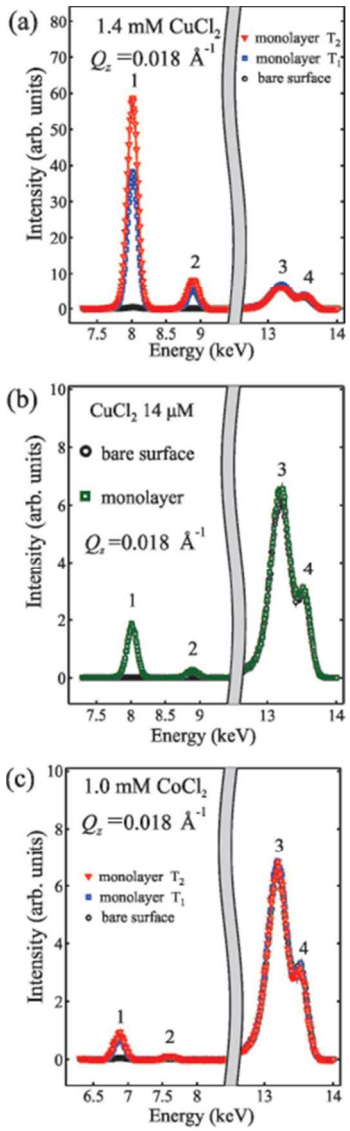

Figure 4. Surface fluorescence spectra obtained at Q_z = 0.018 Å^{-1} for a 1.4 × 10^{-3} M aqueous $CuCl_2$ solution (a), 1.4 × 10^{-5} M $CuCl_2$ solution (b), and for a 10^{-3} M aqueous $CoCl_2$ solution (b) in the presence and absence of the monolayer of **1**. In (a) - (c), a shaded band blocks the unessential spectral portion for

display purpose. In (a) and (c), two measurements were sequentially performed at an earlier time T_1 and a later time T_2 on the same sample surface, with a time interval (T_2 - T_1) of ~ 1 h. Numerical labels 1 and 2 denote Kα and Kβ emission lines respectively from surface ions (Cu^{2+} or Co^{2+}). Label 3 denotes the Compton (inelastic) scattering and label 4 the Thomson (elastic) scattering. 3 and 4 result from the interaction of X-rays and water and helium gas. In (a) - (c), the error bars are smaller than the data symbol size.

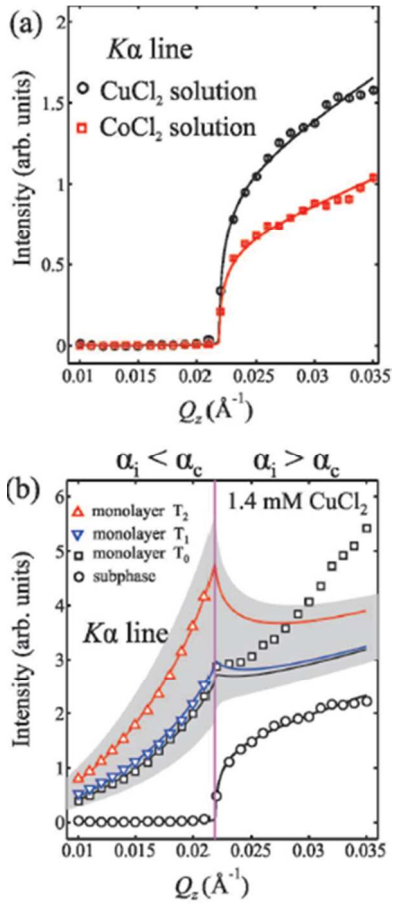

Figure 5: Angular dependences of fluorescence intensity of the Kα emission line (integrated over the energy band width of 0.8 keV) from bulk aqueous ions of Cu^{2+} and Co^{2+}, both of which are normalized to the concentration of 10^{-3} M. (b) Angular dependence of fluorescence intensity of the Kα emission line from 1.4 × 10^{-3} M aqueous $CuCl_2$ solutions with and without the monolayer of **1** on the surface as indicated. The vertical dashed line indicates the Q_c. The data (labeled as an earlier time T_1 and later time

T_2) were measured only below the critical angle and were corrected for different beam attenuation levels, relative to the full Q_z-scans, for the bare surface solution and monolayer-covered solution (labeled T_0). In both (a) and (b), the error bars are smaller than the data symbol size.

For a 1.4×10^{-3} M $CuCl_2$ or a 10^{-3} M $CoCl_2$ (and for 10^{-5} M of both ions) in the absence of Langmuir film, the Cu and Co emission lines are barely detectable at $Q_z = 0.018$ Å^{-1} as the density of the Cu^{2+} or Co^{2+} ions within the penetration depth near surface is below the detection limit of the instrument. However, in the presence of the monolayer of **1**, the specific emission lines of the ions are readily visible, indicating a surface enrichment of both ions. The photon signals arising from the scattering of the primary beam from water surface and the water-saturated helium vapor are also visible (Thomson and Compton around 13.4 keV), as shown in Figure 4, and their intensities serve for normalization purposes between different experiments. For each sample, a series of fluorescence measurements were repeated at time intervals of ~ 20 - 60 minutes showing time-dependent accumulation of surface Cu^{2+}. For similar concentrations, the intensity of the emission lines of Cu^{2+} are almost 25 to 38 times those of Co^{2+}, a direct evidence for significantly stronger affinity for Cu^{2+} carboxylic template formed by **1**. Even for Cu^{2+} ions at extremely low concentration, the fluorescence data unambiguously show that there is surface binding of copper at a bulk concentration of 1.4×10^{-5} M, as seen in Figure 4. By comparing the relative intensity values, the surface excess of Cu^{2+} ions is approximately 20 - 30 times lower than that observed on a 1.4×10^{-3} M $CuCl_2$ subphase, and it is comparable to the surface excess of Co^{2+} ions on a 10^{-3} M aqueous $CoCl_2$ subphase.

We note that with our set-up, the ratio between the intensity of Kα from Cu^{2+} and Co^{2+} ions of equivalent amount is about 1.6 based on analysis of Figure 5, as discussed below. Moreover, the emission line intensities for surface-bound Cu^{2+} ions increase over time, suggesting a persistent

surface aggregation of the ions, in contrast to the time-independence for surface-bound Co^{2+} ions. We argue that the time-dependent enhancement is not induced by X-ray irradiation as it is observed for Cu^{2+} ions but not for Co^{2+} ions, under practically identical conditions and within similar time scales.

To quantify the amount of the surface-bound ions, fluorescence measurements for bulk ion solutions of known concentrations were also performed. Figure 5 shows the angular dependence of the fluorescence intensity (integrated over the Kα emission line) for the aqueous $CuCl_2$ and $CoCl_2$ solutions normalized to the same concentration, *i.e.* 10^{-3} M, both with a bare surface. The intensity at each incident angle (and equivalently each Q_z), I_{bulk} (α_i), can be profile-fit with the equation

$$I_{bulk}(\alpha_i) = CT(\alpha_i)D(\alpha_i)n_{bulk} \qquad (1)$$

where $T(\alpha_i)$ and $D(\alpha_i)$ are the Fresnel intensity transmission function[34] and the penetration depth function normal to the surface, respectively.[35] n_{bulk} is the known concentration of the aqueous ions solution. For the same scattering geometry in all fluorescence measurements, the scaling factor C, after normalization to the incident beam intensity, depends on the efficiency of the detector for photons of different energies and elemental fluorescence yields, thus being element specific. It is found that the ratio of C of Cu^{2+} to Co^{2+} is 1.6, for the same bulk concentration of ions.

The Q_z-dependence of fluorescence intensities in Figure 5 is shown for a 1.4×10^{-3} M aqueous $CuCl_2$ subphase in the absence of the monolayer of **1**, and in the presence of the monolayer but measured sequentially at time T_0, T_1 and T_2, with $T_0 < T_1 < T_2$, and time separation of ~ 30 minutes to 1 hour. The surface fluorescence intensity is given by

$$I_{\text{surface}}(\alpha_i) = CT(\alpha_i) n_{\text{surface}} \exp\left(-|z_{\text{ion}}| / D(\alpha_i)\right) \qquad (2)$$

where z_{ion} is the position of a thin ion enriched layer beneath the air-layer interface (z = 0) and n_{surface} represents the surface excess number of ions per unit of area. It is found that the intensities at $\alpha_i < \alpha_c$ can be profile-fit with Eq. (2), where the best-fit parameters give $z_{\text{ion}} \approx$ - 11 and - 16 Å and $n_{\text{surface}} \approx 0.03$ and 0.05 Å^{-2} for data collected at T_1 and T_2, respectively. The shaded area in Figure 6 is calculated by Eq. (1) and (2) with lower boundary corresponding to z_{ion} = - 10 Å and n_{surface} = 0.02 Å^{-2} and upper boundary corresponding to z_{ion} = - 20 and n_{surface} = 0.06 Å^{-2}, thus providing a semi-quantitative estimate of the surface ion population and a prediction of the fluorescence intensity beyond α_c. Using the molecular area ~ 115 Å^2 obtained from the isotherms we obtain 4.6 ± 1.2 Cu^{2+} per molecule of **1**, equivalent to 1.2 ± 0.3 Cu^{2+} per carboxylic group. Similar analysis for the monolayer of **1** on Co^{2+} yields $n_{\text{surface}} \sim 0.001$ Å^{-2} or 0.15 Co^{2+} per molecule of **1**. For $\alpha_i > \alpha_c$, Q_z-scan data deviate from the model prediction based on the data collected below Q_c (solid lines in Figure 5). The shaded area, containing the data collected only below Q_c, provides an estimate of the surface excess of the Cu^{2+} ions based on the simplistic surface Cu^{2+} ions enrichment model, *i.e.* Eq. (1) and (2), and further predicts the fluorescence data expected above Q_c. In general, in a full Q_z fluorescence scan, a thin layer of surface fluorescing ions gives rise to a surface enhancement near $Q_z = Q_c$ due to the evanescence effect. This fluorescence enhancement levels off for $Q_z > Q_c$, as the X-rays penetrate deeper into the bulk. These features can be observed in similar studies of specific, fluorescing elemental surface excess in the presence of charged monolayers on aqueous surfaces.[36] The apparent upturn of the fluorescence intensity with Q_z is anomalous and fails to be accounted for by this simple model. This anomaly has been observed repeatedly and it is specific to the fluorescence data collected at $\alpha_i > \alpha_c$ for the **1**-$CuCl_2$ system when X-rays penetrate into the bulk. It can be qualitatively

attributed to the formation of non-uniform (of time-dependent sizes) clusters of Cu^{2+} ions in the bulk that interact with the monolayer.

The reflectivity data, $R(Q_z)$, are normalized to the calculated Fresnel reflectivity, R_F, of an ideally sharp and flat air-water interface. The R/R_F of **1** on different aqueous subphases and the structural parameters that are used to fit the data are shown in Figure 6 and Table 2, respectively.

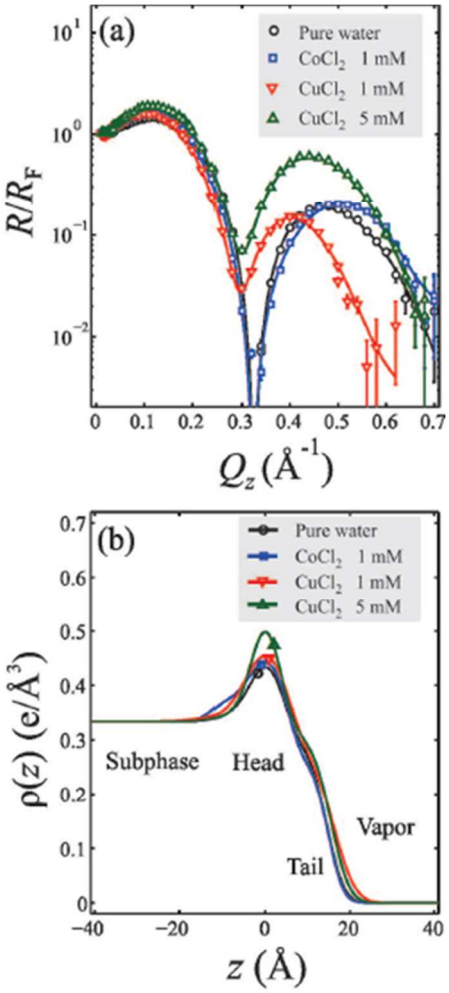

Figure 6. (a) Reflectivity data (R) normalized to the Fresnel reflectivity (R_F), R/R_F, for the monolayer of **1** on water, on 10^{-3} M aqueous $CoCl_2$ and $CuCl_2$ solutions and on a 5×10^{-3} M aqueous $CoCl_2$ solution. (b)

Corresponding best-fit electron density (ED) profiles across the interfaces. The solid lines in (a) through most data points are calculated in terms of the ED profiles in (b).

Table 2. Structural parameters of the monolayer of **1** on various subphase conditions in terms of the reflectivity data analysis.

	Water	$CoCl_2$ (10^{-3} M)	$CuCl_2$ (10^{-3} M)	$CuCl_2$ (5×10^{-3} M)
d_1 (Å)	7.3 ± 0.6	9.1 ± 0.8	12 ± 3	8.2 ± 0.8
ρ_1 (e/Å^3)	0.353 ± 0.007	0.381 ± 0.004	0.35 ± 0.03	0.35 ± 0.01
d_2 (Å)	7 ± 2	7 ± 2	10 ± 2	8 ± 2
ρ_2 (e/Å^3)	0.49 ± 0.04	0.49 ± 0.04	0.48 ± 0.05	0.54 ± 0.04
d_3 (Å)	10.6 ± 0.7	10.1 ± 0.6	11.0 ± 1.0	11.4 ± 0.8
ρ_3 (e/Å^3)	0.29 ± 0.01	0.26 ± 0.01	0.27 ± 0.04	0.27 ± 0.02
σ (Å)	3.2 ± 0.2	3.0 ± 0.2	3.9 ± 0.2	2.9 ± 0.2
Γ^e (e/Å^2)	0.61 ± 0.08	0.75 ± 0.10	0.95 ± 0.24	1.01 ± 0.11
n_{ion}	N/A	0.65 ± 0.60	1.5 ± 1.1	1.7 ± 0.6
$\boldsymbol{\chi^2_{\nu,min}}$	1.3	6.8	2.7	1.9

The reflectivity data are interpreted using a three-box model, where the monolayer ED profile is parsed into three boxes (or layers) along the surface normal. Three pairs of values, (ρ_1, d_1), (ρ_2, d_2), and (ρ_3, d_3) refer to the ED and the thickness for each layer of the strata on the aqueous surface with the subscript 3 and 1 denoting the top and bottom layer in direct contact with the vapor phase and the aqueous subphase, respectively. The common interfacial roughness is denoted by σ.[34] The surface excess electron density is denoted as Γ^e, which is defined as $\boldsymbol{\Gamma^e} \equiv \sum[(\boldsymbol{\rho_i} - \boldsymbol{\rho}_{sub}) \times \boldsymbol{d_i}]$, ($i$ = 1, 2, 3), and ρ_{sub} represents the electron density of the aqueous subphase (0.334 e/Å^3). The number of surface bound metal cations (Cu^{2+} or Co^{2+}) per molecule is denoted as n_{ion}. Using a space-filling model,[37] n_{ion} can be estimated based on the molecular area A_0 (115 ± 5 Å^2 molecule^{-1} for the monolayer of **1** compressed at a surface pressure of 20 mN m^{-1}, in terms of the isotherm data), surface electron excess Γ^e, and the cationic volume (denoted as v_{ion} and calculated using the tabulated ionic radii, 0.74 Å for Cu^{2+} and 0.65 Å for Co^{2+}), that is, $n_{ion} = \Delta(A_0\Gamma^e)/(N^e_{ion} - \rho_{sub}v_{ion})$ where $\Delta(A_0\Gamma^e)$ is the difference of $(A_0\Gamma^e)$ for the monolayer of **1** on pure water and on the subphase containing metal ioins. N^e_{ion} is the number of electrons in a single cation (27 for Cu^{2+} and 25 for Co^{2+}, respectively). Details of the calculation of n_{ion} in terms of the structural parameters can be found elsewhere.[36,38] The refinement of the reflectivity data was carried out using the Parratt's exact recursive method.[34] The quality of the profile fitting was measured with the reduced χ^2, namely, $\boldsymbol{\chi^2_\nu}$. The multi-dimensional parameter space was sampled through the Monte-Carlo method.[39] The ranges of the structural parameters given in the table correspond to an increase in $\boldsymbol{\chi^2_\nu}$ from its minimum, $\boldsymbol{\chi^2_{\nu,min}}$, by no more than 100%. Note that the reflectivity measurements were performed prior to fluorescence and GID measurements and therefore the number of ions per molecule may be fewer than those extracted from fluorescence data because of potential time-dependent binding.

One qualitative feature in the R/R_F data is the first reflectivity minimum position in Q_z, denoted as Q'_z. A simple rule, developed by Kjaer,[40] states that $Q'_z \approx 3\pi\ (l_H + 2l_T)^{-1}$, where l_H and l_T represent the thickness of the hydrophilic head group and hydrophobic tail group of the film, respectively. Figure 6 shows that $Q'_z \approx 0.33$ Å^{-1}, corresponding to $(l_H/2 + l_T) \approx 14.3$ Å, for R/R_F data of the monolayer of **1** on pure water. In the presence of a 10^{-3} M aqueous $CoCl_2$ solution, the value of Q'_z barely changes, indicating weak or even non-cationic binding. In contrast, in the presence of a 10^{-3} M aqueous $CuCl_2$ solution, the Q'_z shifts to a lower value ~ 0.3 Å^{-1}, corresponding to $(l_H/2 + l_T) \approx 15.7$ Å, *i.e.* a thicker monolayer. Further increase of the bulk $CuCl_2$ concentration barely changes the value of Q'_z, suggesting that the monolayers are approaching saturation of ion binding. Figure 6 shows the corresponding electron-density (ED) profiles constructed in terms of best-fit structural parameters (Table 2). From the left to the right, four regions are readily associated with the subphase, head groups, tail groups, and vapor phase.

Based on the structural parameters extracted from reflectivity analysis, the binding ratio of surface bound cations (Cu^{2+} or Co^{2+}) per molecule of **1**, denoted as n_{ion}, can be evaluated. Using a space-filling model,[37] n_{ion} can be estimated based on the molecular area A (~ 115 Å^2 for all subphases), surface electron excess Γ^e (see Table 2) and the cationic volume (denoted as v_{ion} and calculated using the tabulated ionic radii, 0.74 Å for Cu^{2+} and 0.65 Å for Co^{2+} ions. Details of the calculation of n_{ion} in terms of the structural parameters can be found in the footnote of the Table 2 and elsewhere.[36,38] For copper, the reflectivity results suggest an average of 1.5 ± 1.1 Cu^{2+} per molecule of **1** (for a 10^{-3} M aqueous $CuCl_2$ subphase), which is near the lower bound of the stoichiometric ratio extracted from the fluorescence results. For Co^{2+} ions, the reflectivity evidence for surface binding is relatively weak due to the estimate value (0.65 Co^{2+} per molecule) is comparable to the associated error (± 0.60 Co^{2+} per molecule). Nevertheless, the

binding ratio estimated from fluorescence (0.15 ± 0.04 Co^{2+} per molecule) falls within the range provided by the reflectivity analysis.

The GIXD scans integrated over Q_z as a function of Q_{xy}, cf. Figure 7, were performed in the attempt to look for possible ordering of the Cu-headgroup and determine the formed complexes at the interface. However, as discussed below, we only observed diffraction peaks from the hydrocarbon chains and water.

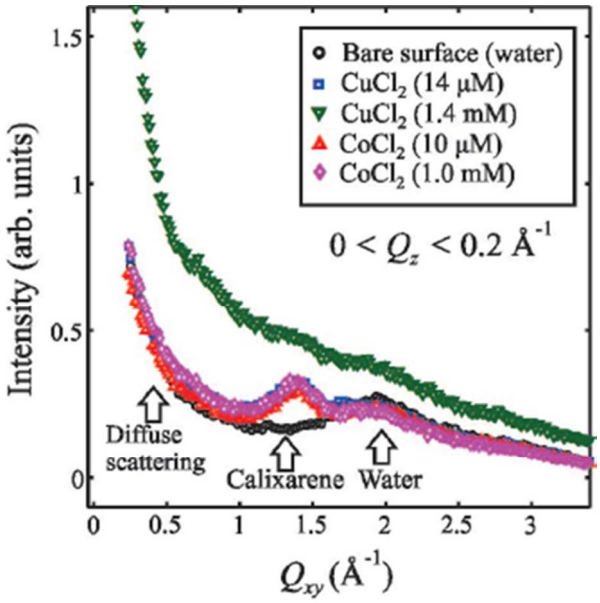

Figure 7. Integrated GIXD data over Q_z = 0 - 0.2 $Å^{-1}$ as a function of Q_{xy} at α_i = 0.065°. The symbols represent the integrated diffraction intensity from a bare surface of water (circles), from the monolayer of **1** on 1.4 × 10^{-5} M (squares) and 1.4 × 10^{-3} M (downward triangles) aqueous $CuCl_2$ solutions, and on 10^{-5} M (upper triangles) and 10^{-3} M (diamonds) aqueous $CoCl_2$ solutions, respectively.

For a bare water surface, the GIXD intensity is a superposition of a diffuse scattering due to capillary that falls off with Q_{xy} and water structure factor with a prominent peak centered between 1.9 and 2.0 $Å^{-1}$.[28] In the presence of the monolayer of **1** compressed at 20 mN m^{-1}, an additional broad peak emerges at ~ 1.4 $Å^{-1}$ due to liquid-like phase of the hydrocarbon chains as

previously observed.[27] However, as shown in Figure 7, high bulk concentrations of Cu^{2+} ions (1.4×10^{-3} M) dramatically change the GIXD pattern over the entire measured Q_{xy} range. We emphasize that for these high Cu^{2+} concentrations, the GIXD is much more intense though it does not yield the exact same pattern for different preparations. This suggests sporadic non-uniform Cu^{2+} clusters form contiguous to the monolayer making the surface rougher and enhancing the diffuse scattering over the whole Q_{xy} range. This is consistent with the anomalous behavior of the fluorescence discussed above. More studies are necessary to fully determine the details of this anomaly.

CONCLUSIONS

The interactions of Langmuir monolayers of **1** with the divalent fourth-period transition-metal ions Cu^{2+}, Co^{2+}, Mn^{2+} and Ni^{2+} were investigated by means of Langmuir compression isotherms, BAM, and surface sensitive X-ray scattering methods. The data indicate that the macroscopic and microscopic structure of the monolayer of **1** is considerably affected by Cu^{2+} ions, suggesting a strong interaction of this transition metal ion with the monolayer. Quantitative X-ray fluorescence measurements near the critical angle for total reflection show significant amount of bound Cu^{2+} ions beyond what would be necessary to bind the four carboxylic groups of **1**. Furthermore, the various X-ray results strongly suggest that Cu(II)-hydroxide clusters form deep below the monolayer. In contrast, Co^{2+} ions at similar concentrations bind to the monolayer at a surface density about 30 times lower than that of Cu^{2+} ions. The binding and cluster formation of Cu(II)-hydroxide is found to be strongly time-dependent such that, within the time frame of experiments (from 1 to 3 hours), Cu^{2+} ions continuously accumulate beneath the monolayer.

ASSOCIATED CONTENT

Supporting Information

BAM micrographs of the monolayer of **1** on aqueous $CuCl_2$, $CoCl_2$, $NiCl_2$ and $MnCl_2$ subphases, XRR and XNTRF data analysis. This material is available free of charge via the Internet at http://pubs.acs.org.

AUTHOR INFORMATION

Corresponding Author

* E-mail: patrick.shahgaldian@fhnw.ch

Tel: +41 61 467 43 46

Author contributions

The manuscript was written through contributions of all authors. All authors have given approval to the final version of the manuscript.

Notes

The authors declare no competing financial interest.

ACKNOWLEDGMENTS

The financial support from the Swiss Nanoscience Institute (SNI, grant NanoMorph) and the Swiss National Science Foundation (SNSF, grant CalixCargo 2) is gratefully acknowledged. The work at the Ames Laboratory is supported by the Office of Basic Energy Sciences, U.S. Department of Energy under Contract No DEAC02-07CH11358. X-ray diffraction at the

Advanced Photon Source is supported by the U.S. Department of Energy, Basic Energy Sciences, Office of Science, under Contract No. DE-AC02-06CH11357.

REFERENCES

1. Zhang, X.; Wang, C. Supramolecular amphiphiles. *Chem. Soc. Rev.* **2011,** *40*, 94-101.
2. Chen, G.; Jiang, M. Cyclodextrin-based inclusion complexation bridging supramolecular chemistry and macromolecular self-assembly. *Chem. Soc. Rev.* **2011,** *40*, 2254-2266.
3. Zhao, X.; Pan, F.; Xu, H.; Yaseen, M.; Shan, H.; Hauser, C. A. E.; Zhang, S.; Lu, J. R. Molecular self-assembly and applications of designer peptide amphiphiles. *Chem. Soc. Rev.* **2010,** *39*, 3480-3498.
4. Palmer, L. C.; Stupp, S. I. Molecular Self-Assembly into One-Dimensional Nanostructures. *Acc. Chem. Res.* **2008,** *41*, 1674-1684.
5. Wang, C.; Wang, Z.; Zhang, X. Amphiphilic Building Blocks for Self-Assembly: From Amphiphiles to Supra-amphiphiles. *Acc. Chem. Res.* **2012,** *45*, 608-618.
6. Bilensoy, E. Nanoparticulate Delivery Systems Based on Amphiphilic Cyclodextrins. *J. Biomed. Nanotechnol.* **2008,** *4*, 293-303.
7. Gokel, G. W.; Leevy, W. M.; Weber, M. E. Crown Ethers: Sensors for Ions and Molecular Scaffolds for Materials and Biological Models. *Chem. Rev.* **2004,** *104*, 2723-2750.
8. Helttunen, K.; Shahgaldian, P. Self-assembly of amphiphilic calixarenes and resorcinarenes in water. *New J. Chem.* **2010,** *34*, 2704-2714.
9. Gutsche, C. D.; Dhawan, B.; No, K. H.; Muthukrishnan, R. Calixarenes. 4. The synthesis, characterization, and properties of the calixarenes from p-tert-butylphenol. *J. Am. Chem. Soc.* **1981,** *103*, 3782-3792.
10. Izatt, R. M.; Lamb, J. D.; Hawkins, R. T.; Brown, P. R.; Izatt, S. R.; Christensen, J. J. Selective M+-H+ coupled transport of cations through a liquid membrane by macrocyclic calixarene ligands. *J. Am. Chem. Soc.* **1983,** *105*, 1782-1785.

11. Gale, P. A.; Haynes, C. J. E. Anion Receptors Containing Heterocyclic Rings. In *Supramolecular Chemistry: From Molecules to Nanomaterials*; Gale, P. A., Steed, J. W. Eds.; John Wiley & Sons, Ltd: 2012; pp 1125-1152.

12. Gale, P. A.; Sessler, J. L.; Král, V.; Lynch, V. Calix[4]pyrroles: Old Yet New Anion-Binding Agents. *J. Am. Chem. Soc.* **1996,** *118*, 5140-5141.

13. Diamond, D.; McKervey, M. A. Calixarene-based sensing agents. *Chem. Soc. Rev.* **1996,** *25*, 15-24.

14. Böhmer, V.; Dalla Cort, A.; Mandolini, L. Counteranion Effect on Complexation of Quats by a Neutral Calix[5]arene Receptor. *J. Org. Chem.* **2001,** *66*, 1900-1902.

15. Colasson, B.; Poul, N. L.; Mest, Y. L.; Reinaud, O. Electrochemically Triggered Double Translocation of Two Different Metal Ions with a Ditopic Calix[6]arene Ligand. *J. Am. Chem. Soc.* **2010,** *132*, 4393-4398.

16. Ikeda, A.; Shinkai, S. On the Origin of High Ionophoricity of 1,3-Alternate Calix[4]arenes: .pi.-donor Participation in Complexation of Cations and Evidence for Metal-Tunneling through the Calix[4]arene Cavity. *J. Am. Chem. Soc.* **1994,** *116*, 3102-3110.

17. Leray, I.; Valeur, B. Calixarene-Based Fluorescent Molecular Sensors for Toxic Metals. *Eur. J. Inorg. Chem.* **2009,** *2009*, 3525-3535.

18. Markowitz, M. A.; Bielski, R.; Regen, S. L. Ultrathin monolayers and vesicular membranes from calix[6]arenes. *Langmuir* **1989,** *5*, 276-278.

19. Shahgaldian, P.; Cesario, M.; Goreloff, P.; Coleman, A. W. Para-acyl calix[4]arenes: amphiphilic self-assembly from the molecular to the mesoscopic level. *Chem. Commun.* **2002**, 326-327.

20. Vollhardt, D.; Gloede, J.; Weidemann, G.; Rudert, R. Characteristic Features of Amphiphilic P-Functionalized Calixarene Monolayers at the Air/Water Interface. *Langmuir* **2003,** *19*, 4228-4234.

21. Nakamoto, Y.; Kallinowski, G.; Boehmer, V.; Vogt, W. Langmuir monolayers of p-octadecylcalix[4]arene. *Langmuir* **1989,** *5*, 1116-1117.

22. Markowitz, M. A.; Bielski, R.; Regen, S. L. Perforated monolayers: porous and cohesive monolayers from mercurated calix[6]arenes. *J. Am. Chem. Soc.* **1988,** *110*, 7545-7546.

23. Ishikawa, Y.; Kunitake, T.; Matsuda, T.; Otsuka, T.; Shinkai, S. Formation of calixarene monolayers which selectively respond to metal ions. *J. Chem. Soc., Chem. Commun.* **1989**, 736-738.

24. Shahgaldian, P.; Coleman, A. W. Anion and Cation Interactions with p-Dodecanoylcalix[4]arene Monolayers at the Air−Water Interface. *Langmuir* **2001,** *17*, 6851-6854.

25. Lonetti, B.; Fratini, E.; Casnati, A.; Baglioni, P. Langmuir monolayers of calix[8]arene derivatives: complexation of alkaline earth ions at the air/water interface. *Colloids Surf. A* **2004,** *248*, 135-143.

26. Lonetti, B.; Lo Nostro, P.; Ninham, B. W.; Baglioni, P. Anion Effects on Calixarene Monolayers: A Hofmeister Series Study. *Langmuir* **2005,** *21*, 2242-2249.

27. Tulli, L. G.; Moridi, N.; Wang, W.; Helttunen, K.; Neuburger, M.; Vaknin, D.; Meier, W.; Shahgaldian, P. Polymorphism control of an active pharmaceutical ingredient beneath calixarene-based Langmuir monolayers. *Chem. Commun.* **2014,** *50*, 3938-3940.

28. Wang, W.; Murthy, N. S.; Kuzmenko, I.; Anderson, N. A.; Vaknin, D. Structure of Biodegradable Films at Aqueous Surfaces: X-ray Diffraction and Spectroscopy Studies of Polylactides and Tyrosine-Derived Polycarbonates. *Langmuir* **2013,** *29*, 11420-11430.

29. Ye, B.-H.; Tong, M.-L.; Chen, X.-M. Metal-organic molecular architectures with 2,2′-bipyridyl-like and carboxylate ligands. *Coord. Chem. Rev.* **2005,** *249*, 545-565.

30. Plater, M. J.; St J. Foreman, M. R.; Howie, R. A.; Skakle, J. M. S.; Slawin, A. M. Z. Hydrothermal synthesis of polymeric metal carboxylates from benzene-1,2,4,5-tetracarboxylic acid and benzene-1,2,4-tricarboxylic acid. *Inorg. Chim. Acta* **2001,** *315*, 126-132.

31. Eremenko, I. L.; Nefedov, S. E.; Sidorov, A. A.; Golubnichaya, M. A.; Danilov, P. V.; Ikorskii, V. N.; Shvedenkov, Y. G.; Novotortsev, V. M.; Moiseev, I. I. Bi- and Mononuclear Nickel(II) Trimethylacetate Complexes with Pyridine Bases as Ligands. *Inorg. Chem.* **1999,** *38*, 3764-3773.

32. Liu, G.-F.; Ye, B.-H.; Ling, Y.-H.; Chen, X.-M. Interlocking of molecular rhombi into a 2D polyrotaxane network *via* π-π interactions. Crystal structure of [Cu2(bpa)2(phen)2(H2O)]2•2H2O (bpa2- = biphenyl-4,4'-dicarboxylate, phen = 1,10-phenanthroline). *Chem. Commun.* **2002**, 1442-1443.

33. González-Delgado, A. M.; Giner-Casares, J. J.; Brezesinski, G.; Regnouf-de-Vains, J.-B.; Camacho, L. Langmuir Monolayers of an Inclusion Complex Formed by a New Calixarene Derivative and Fullerene. *Langmuir* **2012,** *28*, 12114-12121.

34. Als-Nielsen, J.; McMorrow, D. Refraction and reflection from interfaces. In *Elements of Modern X-ray Physics*; John Wiley & Sons: 2011; pp 69-112.

35. Vaknin, D. X-Ray Diffraction and Spectroscopic Techniques for Liquid Surfaces and Interfaces. In *Characterization of Materials*; Kaufmann, E. N. Eds.; John Wiley & Sons: New York: 2012; pp 1-32.

36. Wang, W.; Anderson, N. A.; Travesset, A.; Vaknin, D. Regulation of the Electric Charge in Phosphatidic Acid Domains. *J. Phys. Chem. B* **2012,** *116*, 7213-7220.

37. Vaknin, D. X-Ray Diffraction and Spectroscopic Techniques for Liquid Surfaces and Interfaces. In *Characterization of Materials*; Kaufmann, E. N. Eds.; John Wiley & Sons: New York: 2012; pp 1393-1423.

38. Wang, W.; Pleasants, J.; Bu, W.; Park, R. Y.; Kuzmenko, I.; Vaknin, D. Amorphous iron-(hydr) oxide networks at liquid/vapor interfaces: In situ X-ray scattering and spectroscopy studies. *J. Colloid Interface Sci.* **2012,** *384*, 45-54.

39. Wang, W.; Bu, W.; Wang, L.; Palo, P. E.; Mallapragada, S.; Nilsen-Hamilton, M.; Vaknin, D. Interfacial Properties and Iron Binding to Bacterial Proteins That Promote the Growth of Magnetite Nanocrystals: X-ray Reflectivity and Surface Spectroscopy Studies. *Langmuir* **2012,** *28*, 4274-4282.

40. Kjaer, K. Some simple ideas on X-ray reflection and grazing-incidence diffraction from thin surfactant films. *Phys. B (Amsterdam, Neth.)* **1994,** *198*, 100-109.

TOC Graphic

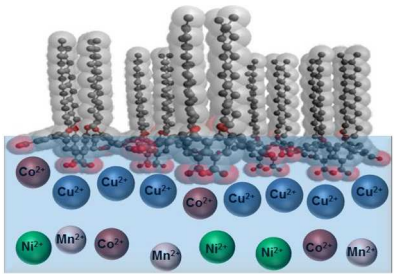
Co2+
Cu2+
Cu2+
Cu2+
Co2+
Cu2+
Cu2+
Cu2+
Cu2+
Ni2+
Mn2+
Co2+
Mn2+
Ni2+
Ni2+
Co2+
Mn2+